Auger decay and the direct double ionization probability of a 2p inner-shell hole in a singly charged Ar+ ion

Article *in* The European Physical Journal D · August 2014

Impact Factor: 1.23 · DOI: 10.1140/epjd/e2014-50124-5

4 authors, including:

Jianmin Yuan
National University of Defense Technology
233 PUBLICATIONS **1,858** CITATIONS

EPJ D
Atomic, Molecular, Optical and Plasma Physics
EPJ.org
your physics journal

Eur. Phys. J. D (2014) 68: 214 DOI: 10.1140/epjd/e2014-50124-5

Auger decay and the direct double ionization probability of a 2p inner-shell hole in a singly charged Ar^+ ion

Pengfei Liu, Yanpeng Liu, Jiaolong Zeng and Jianmin Yuan

edp sciences
Società Italiana di Fisica
Springer

Eur. Phys. J. D (2014) 68: 214
DOI: 10.1140/epjd/e2014-50124-5

THE EUROPEAN PHYSICAL JOURNAL D

Regular Article

Auger decay and the direct double ionization probability of a 2p inner-shell hole in a singly charged Ar^+ ion

Pengfei Liu, Yanpeng Liu, Jiaolong Zeng[a], and Jianmin Yuan

Department of Physics, College of Science, National University of Defense Technology, Changsha Hunan 410073, P.R. China

Received 17 February 2014 / Received in final form 13 April 2014
Published online 7 August 2014 – © EDP Sciences, Società Italiana di Fisica, Springer-Verlag 2014

Abstract. Single and double Auger decay processes of Ar^+ $2p^{-1}$ hole levels belonging to the configurations of $2p^53s^23p^5$ and $2p^53s3p^6$ are investigated in the framework of perturbation theory implemented by the distorted wave approximation. The single Auger decay channels and rates are determined and the predicted total rates can differ by more than an order of magnitude for the levels of $2p^53s^23p^5$, yet they are very close for levels belonging to $2p^53s3p^6$. By combining the double photoionization cross sections of the neutral species, our theoretical Auger spectra of the single Auger decay process nicely interpreted a recent experiment [S.M. Huttula et al., Phys. Rev. Lett. **110**, 113002 (2013)]. A configuration averaged branching ratio of 6.5% and 7.3% are predicted for the direct double Auger decay to the total probability for $2p^53s^23p^5$ and $2p^53s3p^6$, respectively, which is smaller than that of Ar $2p^{-1}$ hole states.

1 Introduction

When atoms or molecules absorb extreme ultraviolet or X-ray photons, inner-shell photoionization occurs with the production of inner-shell hole states. The hole states will then decay dominantly by the Auger process for light elements. Knowledge of the Auger decay of the inner-shell hole states is of fundamental interest and an important ingredient for investigating astrophysical and laboratory plasmas [1,2]. However, both the process of the direct double ionization, where two electrons are released simultaneously, and the indirect double photoionization process, in which an excited state is first formed and then decays to a doubly charged ion by autoionization, are studied less. Only with the advent of multicoincidence techniques (such as photoelectron-ion and multielectron coincidence technology) can we directly investigate the indirect double photoionization process. With the utilization of multicoincidence techniques, experimental studies were carried out for the Auger decay including the direct double Auger decay (DDAD) process of the inner-shell vacancy of rare gases [3–7].

However, these experimental investigations are mostly limited to neutral atoms. The inner-shell electronic properties of positively charged ions are basically unexplored due to the experimental difficulty in producing enough density in ionic beams. To the best of our knowledge, only a few researchers or research groups reported such experimental results on the measurement of photoelectron spectra [8–11]. Bizau et al. [8] and Moussalami et al. [9] reported the measurement of photoelectron spectra emitted in the inner-shell photoionization or excitation of Ca^+. Gottwald et al. [10] presented electron spectroscopy in direct $4d$ photoionization of Xe^+ by applying various timing and coincidence techniques to suppress and to monitor on line the strong fluctuating background. Yet no detailed information on the decay of inner-shell hole states was reported for these singly charged ions of Ca^+ and Xe^+. Recently, Huttula et al. [11] experimentally investigated the Auger electron spectroscopy in the decay of a $2p$ inner-shell hole in Ar^+, which was created by the single photon double-ionization of corresponding neutral atom. This method might be extended to study the inner-shell ionization of doubly charged ions. On the other hand, inner-shell hole and/or hollow states of multiply charged ions can be produced by using (soft) X-ray free-electron lasers [12,13]. By employing X-ray radiation as a light source, useful information on electron dynamics can be obtained by monitoring the ion charge states [14–17]. It will become more and more feasible in the future to directly measure the photoelectrons and Auger electrons of ionic species for multiphoton ionization to understand the femtosecond dynamics of such systems [18]. To correctly understand the interactions of ultra-intense X-ray pulses with atoms, one has to know the decay properties of the hole or even hollow states of positively charged ions [19].

In this work, we theoretically investigate the Auger decay of Ar^+ $2p^{-1}$ hole states (levels belonging to the configurations of $2p^53s^23p^5$ and $2p^53s3p^6$), which is helpful to better understand the experimental findings [11]. The DDAD rates are determined to have a more complete understanding of the whole Auger decay process. The probability of cascade double Auger channels is negligibly small compared with that of the DDAD process for these hole

[a] e-mail: jlzeng@nudt.edu.cn

states. The branching ratio (BR) of the DDAD to the total probability is determined according to the level-to-level rates. As far as we know, there are no theoretical investigations reported in the literature on the DDAD process of the inner-shell hole states of positively charged ions. Comparison is made with other experimental and theoretical results wherever available.

2 Theoretical method

The detailed theoretical procedure for the single and double Auger rates was given in recent work [20,21], here we only give an outline in the following. In first order perturbation theory, single Auger decay rate can be written as (in atomic units) [22,23]

$$A^1_{im} = 2\left|\langle\Psi^+_m|\sum_{i<j}^{N}\frac{1}{r_{ij}}|\Psi_i\rangle\right|^2, \quad (1)$$

where $|\Psi_i\rangle$ is the wavefunction of the initial autoionizing level of an ion with charge q and $|\Psi^+_m\rangle$ is the wavefunction of an intermediate level of an ion with charge $q+1$ plus a continuum electron. It is constructed by coupling the wavefunction of the ion state of $(N-1)$ electrons with that of a continuum electron

$$|\Psi^+_m\rangle = \sum_{\kappa}|\Psi_m,\kappa;J_TM_T\rangle, \quad (2)$$

where the intermediate level $|\Psi_m\rangle$ belongs to the quantum state of the atomic system with one less electron than $|\Psi_i\rangle$, J_T is the total angular momentum when the target state is coupled to the free electron, M_T is the projection of the total angular momentum, and κ is the relativistic angular quantum number of the free electron, whose wavefunction is obtained by solving the Dirac equations with the same central potential as that for bound orbitals of $|\Psi_m\rangle$.

The wavefunctions of both the initial autoionizing and intermediate levels are obtained by diagonalizing the relativistic Hamiltonian of respective N-electron and $(N-1)$-electron systems. The basis states ϕ_j, which are referred to as configuration state functions (CSF), are antisymmetric sums of the products of N or $(N-1)$ one-electron Dirac spinors. An atomic state is expressed by a linear combination of CSFs with the same parity

$$\Psi_i(J\pi) = \sum_{j}^{n_c} a_j\phi_j(J\pi), \quad (3)$$

where n_c is the number of CSFs and a_j is the representation of the atomic state in the chosen basis. The total energy $E=\varepsilon_i$ for the initial level and $E=\varepsilon^+_m+k^2_m/2$ for the intermediate level with k_m being the momentum of the Auger electron.

The DDAD rate in second-order perturbation theory reads as:

$$A^2_{if} = \frac{8}{\pi}\int_0^{k_{\max}}\frac{dk_{f1}}{k_{f2}}\times\left|\sum_m\sum_{k_m}\frac{\langle\Psi^{2+}_f|V|\Psi^+_m\rangle\langle\Psi^+_m|V|\Psi_i\rangle}{\varepsilon_i-\varepsilon^+_m-k^2_m/2}\right|^2 \quad (4)$$

where $|\Psi^{2+}_f\rangle$ is the final level of an ion with charge $q+2$ plus two free electrons. The total energy of the final state is conserved with that of the initial level. The summations over the intermediate middle state include a summation over all possible states of the $(q+1)$ ion and a summation over a complete set of bound and continuum states of the remaining electron. To simplify calculations, we employed the approximate formulas obtained according to the knock-out (KO) and shake-off (SO) mechanisms [24]

$$A^2_{KO} = \sum_m A^1_{im}\Omega_{mf}(\varepsilon_0) \quad (5)$$

and

$$A^2_{SO} = \sum_m A^1_{im}|\langle\Psi^{2+}_f|\Psi^+_m\rangle|^2, \quad (6)$$

where $\Omega_{mf}(\varepsilon_0)$ is the electron impact collision strength of the transition from the middle state m to the final state f at the incident energy of ε_0. ε_0 is the Auger electron energy of the first single Auger decay process, which can be determined by the energy conservation law. The matrix element $|\langle\Psi^{2+}_f|\Psi^+_m\rangle|$ is the overlap integral between the two wave functions determined in the field of the intermediate level and in the field of vacancies with two Auger electrons being emitted.

3 Results and discussion

A relativistic approach based on the Dirac equation is utilized in our calculation of the distorted wave approximation implemented by the FAC package [23]. The dominant production of core-valence double photoionization of the neutral Ar atom ([Be] $2p^63s^23p^6$) is Ar^{2+} ions of levels belonging to the configurations of $2p^53s^23p^5$ ($2p^{-1}3p^{-1}$) and $2p^53s3p^6$ ($2p^{-1}3s^{-1}$) of Ar^{2+} with a suitable photon energy around ~300 eV as reported by Huttula et al. [11]. Our focus is to study the Auger decay process after the production of the Ar^+ $2p^{-1}$ hole states. There are 10 levels for the configuration of $2p^53s^23p^5$ and 4 levels for $2p^53s3p^6$ and their assignment is given in Table 1. A jj coupling scheme was used throughout the whole relativistic calculation and the corresponding LS designation is also given for convenience of comparison with other publications in LS coupling. For comparison, the theoretical and experimental results [11,25] for the binding energies and lifetime widths are given to illustrate the status of our understanding. Lablanquie et al. [25] experimentally reported that the Auger decay of the inner-shell $2s$ hole is an efficient way to create multiply charged ions. The authors showed that multi-electron coincidence spectroscopy between the $2s$ photoelectron and all released Auger electrons leads to a complete reconstruction of the Ar $2s$ decay cascade. The first step is dominantly the Coster-Kronig populating Ar^+ $2p^{-1}$ hole states. In order to explain the experiment, Huttula et al. [11] and Lablanquie et al. [25] carried out theoretical calculations within the multi-configuration Dirac-Fock (MCDF) formalism by applying the GRASP92 code [26] and RELCI program from the RATIP package [27] and RELCI extension [28]. Note that the error

Table 1. Binding energies and lifetime widths of Ar^+ $2p^{-1}$ hole states.

	Binding energy (eV)				Lifetime width (meV)		
Level designation	This work	Theory [25]	Expt. [25]	Expt. [11]	This work	Theory [11]	Expt. [11]
$(2p_{3/2}^{-1}3p_{3/2}^{-1})_1$ ($^1P_1$)	279.10	276.954		278.52	20.4	16	20
$(2p_{3/2}^{-1}3p_{3/2}^{-1})_3$ ($^3D_3$)	279.36	277.284	278.9	278.78	13.3	10	30
$(2p_{3/2}^{-1}3p_{1/2}^{-1})_2$ ($^3D_2$)	280.24	278.149	279.9	279.60	41.3	77	80
$(2p_{3/2}^{-1}3p_{1/2}^{-1})_1$ ($^3S_1$)	280.74	278.656	279.9	279.96	59.0	115	80
$(2p_{1/2}^{-1}3p_{1/2}^{-1})_1$ ($^3P_2$)	281.62	279.693	280.4	281.13	14.5	11	15
$(2p_{3/2}^{-1}3p_{3/2}^{-1})_2$ ($^3D_1$)	281.83	279.339	281.2	280.63	298.2	438	200
$(2p_{3/2}^{-1}3p_{3/2}^{-1})_0$ ($^3P_0$)	282.72	280.235	282.5	281.32	307.3	466	200
$(2p_{1/2}^{-1}3p_{3/2}^{-1})_1$ ($^3P_1$)	283.14	280.828	282.5	281.98	257.0	346	200
$(2p_{1/2}^{-1}3p_{3/2}^{-1})_2$ ($^1D_2$)	284.25	281.721	283.3	283.01	275.8	421	200
$(2p_{1/2}^{-1}3p_{1/2}^{-1})_0$ ($^1S_0$)	286.82	283.849	285.3	284.97	269.8	442	250
$(2p_{3/2}^{-1}3s_{1/2}^{-1})_2$ ($^3P_2$)	295.17	291.528	294.3	294.20	134.6	176	80
$(2p_{3/2}^{-1}3s_{1/2}^{-1})_1$ ($^3P_1$)	295.85	292.142	294.9	294.73	136.8	178	200
$(2p_{3/2}^{-1}3s_{1/2}^{-1})_0$ ($^3P_0$)	297.27	293.740			132.0	172	
$(2p_{1/2}^{-1}3s_{1/2}^{-1})_1$ ($^1P_1$)	297.94	294.273	297.0	296.78	137.2	175	200

bars on lifetime widths of the experimental values [11] are estimated to be of ±50%. Our predicted binding energies are in good agreement with the experimental results obtained by Lablanquie et al. [25] and by Huttula et al. [11]. For the lifetime widths, however, evident discrepancy is found between different theoretical results and between the theory and experiment. Interestingly, a good agreement is obtained for the levels with a weak autoionization trend such as $(2p_{3/2}^{-1}3p_{3/2}^{-1})_{1,3}$, and $(2p_{1/2}^{-1}3p_{1/2}^{-1})_1$ between our results and the theoretical and experimental values of Huttula et al. [11]. Reasonable agreement is found for the lifetime widths of the levels belonging to the configuration of $2p^53s3p^6$ between the two theoretical results. Evident difference is, however, found for the levels with a stronger autoionization trend, whose lifetime widths are larger than other levels. For these stronger autoionized levels, the lifetime widths predicted by Huttula et al. [11] are outside the error bars of their experiment, but our values are within the error bars. Both our theory and that of Huttula et al. predicted the level with the largest lifetime width is $(2p_{3/2}^{-1}3p_{3/2}^{-1})_0$, yet Huttula et al. obtained a value larger than our result by 51% and larger than their experimental value by 130%. Similar conclusions apply for the levels of $(2p_{3/2}^{-1}3p_{3/2}^{-1})_{1,2}$, $(2p_{1/2}^{-1}3p_{3/2}^{-1})_2$, and $(2p_{1/2}^{-1}3p_{1/2}^{-1})_0$.

The discrepancy between our results and those theoretical predictions carried out by Huttula et al. [11] are partly due to the different treatment of the electron correlations. Since the Auger decay process is strictly due to electron-electron interaction and hence the CI effect plays an important role in accurately determining the rates [19–21]. In this work, CI calculations were carried out to obtain the Auger decay rates. Single and double excitations from the respective ground configurations of Ar^{2+} and Ar^{3+} to orbitals of $3d$, $4s$, $4p$, and $4d$ are considered for the electron correlations. Taking Ar^{2+} as an example to illustrate the scale of CI. The interactions among the fine-structure levels belonging to the following configurations are included: $2p^63s^23p^4$, $2p^63s^23p^3nl$, $2p^63s3p^5$, $2p^63s3p^4nl$, $2p^63s^23p^2nln'l'$, $2p^63s3p^3nln'l'$, $2p^63p^4nln'l'$, $2p^53s^23p^5$, $2p^53s3p^6$, $2p^53s^23p^4nl$, $2p^53s3p^5nl$, $2p^53s^23p^3nln'l'$, and $2p^53s3p^4nln'l'$ (nl = $3d$, $4s$, $n'l'$ = $3d$, $4s$, $4p$, and $4d$). Similar consideration applies to Ar^{3+} with one less electron. Although the Auger decay channels to levels of $2p$ configurations such as $2p^53s^23p^4$ and $2p^53s3p^5$ of Ar^{3+} are energetically forbidden, it is necessary to include these excited states in the calculation to maintain a balance between the CI of Ar^{2+} and Ar^{3+}. Huttula et al. [11] did not give any details on the scale of CI in their work and thus it is not possible for us to give an analysis of the detailed differences between the two models. The effects of CI on the radiative opacity were systematically investigated for hot dense plasmas [29–32].

There are many autoionizing channels in the fine-structure levels for the decay of Ar^+ $2p^{-1}$ hole states. To simplify the presentation, we give the level-to-configuration Auger decay rates A^1 (s^{-1}) of $2p^53s^23p^5$ and $2p^53s3p^6$ and the corresponding BRs in Table 2. From inspection of this table, one can find that the levels belonging to $2p^53s^23p^5$ dominantly decay to the ground configuration of Ar^{3+} with more than half of the probability except for the levels of $2p_{3/2}^{-1}3p_{3/2}^{-1}$ (J = 1, 3) and $2p_{1/2}^{-1}3p_{1/2}^{-1}$ (J = 1). The next strongest channels are levels belonging to [Ne] $3s3p^4$ and $3p^5$, respectively. For the levels of $2p^53s3p^6$, however, the most pronounced decay channels are due to the configuration of $3s3p^4$ with more than 60% of the total probability. The BR for the cascade double Auger decay is trivial (<1%), which is different from that of Ar $2p^{-1}$ hole states. For levels of Ar $2p^{-1}$, there is a 2.9% probability of the cascade double Auger decay [20]. The decreasing trend of BR with the increasing ionization stage of ions is in general a common feature for

Table 2. Level-to-configuration single Auger decay rates A^1 (s^{-1}) for the main channels of Ar^+ $2p^{-1}$ hole states. Figures in brackets indicate powers of ten. The first three columns refer to the initial $2p^{-1}v_s^{-1}(v_s = 3s, 3p)$ level, angular momentum J and final configuration designation, respectively, and the last two columns to the single Auger decay rates and BRs (in %) obtained in this work.

Level	J	Final config.	A^1	BR (%)
$2p_{3/2}^{-1}3p_{3/2}^{-1}$	1	$3s^23p^3$	1.079 (13)	34.9
		$3s3p^4$	6.355 (12)	20.5
		$3p^5$	3.713 (12)	12.0
		$3s^23p^23d$	4.645 (12)	14.4
		$3s3p^33d$	1.800 (12)	5.8
$2p_{3/2}^{-1}3p_{3/2}^{-1}$	3	$3s^23p^3$	6.589 (12)	32.7
		$3s3p^4$	2.595 (12)	12.9
		$3p^5$	2.804 (12)	13.9
		$3s^23p^23d$	1.066 (12)	5.3
		$3s3p^33d$	2.962 (12)	14.7
$2p_{3/2}^{-1}3p_{1/2}^{-1}$	2	$3s^23p^3$	3.619 (13)	57.7
		$3s3p^4$	9.993 (12)	15.9
		$3p^5$	3.643 (12)	5.8
		$3s^23p^23d$	4.639 (12)	7.4
$2p_{3/2}^{-1}3p_{1/2}^{-1}$	1	$3s^23p^3$	5.452 (13)	60.8
		$3s3p^4$	1.606 (13)	17.9
		$3p^5$	3.860 (12)	4.3
		$3s^23p^23d$	7.067 (12)	7.9
$2p_{1/2}^{-1}3p_{1/2}^{-1}$	1	$3s^23p^3$	7.187 (12)	32.6
		$3s3p^4$	3.469 (12)	15.7
		$3p^5$	3.089 (12)	14.0
		$3s^23p^23d$	1.897 (12)	8.6
		$3s3p^33d$	1.881 (12)	8.5
		$3s^23p3d^2$	1.786 (12)	8.1
$2p_{3/2}^{-1}3p_{3/2}^{-1}$	2	$3s^23p^3$	3.098 (14)	68.4
		$3s3p^4$	8.062 (13)	17.8
		$3s^23p^23d$	3.949 (13)	8.5
$2p_{3/2}^{-1}3p_{3/2}^{-1}$	0	$3s^23p^3$	3.181 (14)	68.1
		$3s3p^4$	7.871 (13)	16.9
		$3s^23p^23d$	3.949 (13)	8.5
$2p_{1/2}^{-1}3p_{3/2}^{-1}$	1	$3s^23p^3$	2.655 (14)	68.0
		$3s3p^4$	6.672 (13)	17.1
		$3s^23p^23d$	3.029 (13)	7.8
$2p_{1/2}^{-1}3p_{3/2}^{-1}$	2	$3s^23p^3$	2.835 (14)	67.7
		$3s3p^4$	7.88 (13)	18.8
		$3s^23p^23d$	2.607 (13)	6.2
$2p_{1/2}^{-1}3p_{1/2}^{-1}$	0	$3s^23p^3$	2.639 (14)	64.4
		$3s3p^4$	9.520 (13)	23.2
		$3s^23p^23d$	3.097 (13)	7.6
$2p_{3/2}^{-1}3s_{1/2}^{-1}$	2	$3s3p^4$	1.497 (14)	73.2
		$3p^5$	2.018 (13)	9.9
		$3s^23p^23d$	8.746 (12)	4.3
		$3s3p^33d$	1.334 (13)	6.52
$2p_{3/2}^{-1}3s_{1/2}^{-1}$	1	$3s3p^4$	1.416 (14)	68.1
		$3p^5$	2.199 (13)	10.6
		$3s^23p^23d$	2.408 (13)	11.6
$2p_{3/2}^{-1}3s_{1/2}^{-1}$	0	$3s3p^4$	1.463 (14)	72.9
		$3p^5$	2.853 (13)	14.2
		$3s^23p^23d$	9.466 (12)	4.7
$2p_{1/2}^{-1}3s_{1/2}^{-1}$	1	$3s3p^4$	1.319 (14)	63.3
		$3p^5$	1.137 (13)	5.5
		$3s^23p^23d$	3.737 (13)	17.9

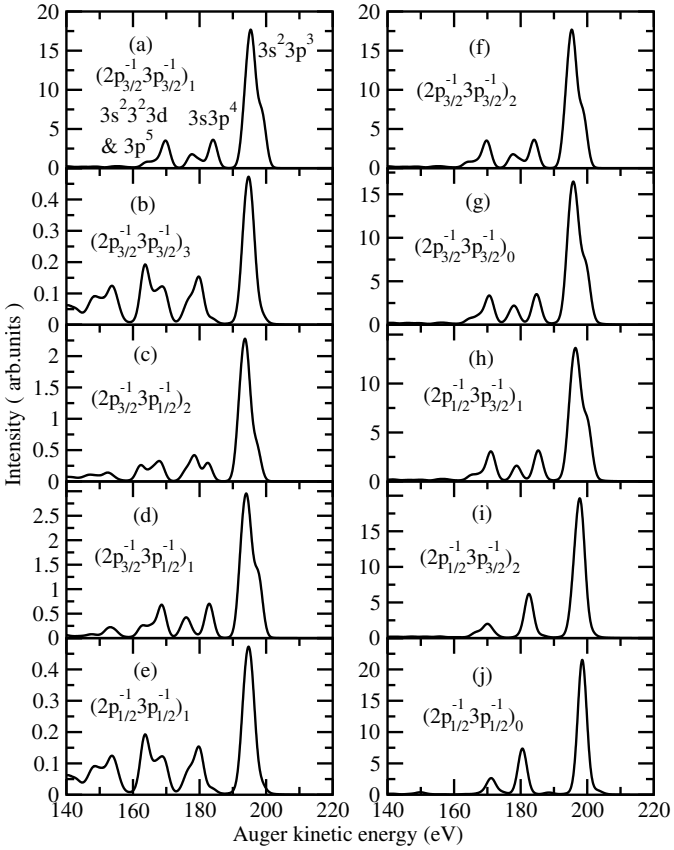

Fig. 1. Auger spectra for the single Auger decay of levels belonging to Ar^{2+} $2p^53s^23p^5$ $(2p^{-1}3p^{-1})$ configuration: (a) $(2p_{3/2}^{-1}3p_{3/2}^{-1})_1$, (b) $(2p_{3/2}^{-1}3p_{3/2}^{-1})_3$, (c) $(2p_{3/2}^{-1}3p_{1/2}^{-1})_2$, (d) $(2p_{3/2}^{-1}3p_{1/2}^{-1})_1$, (e) $(2p_{1/2}^{-1}3p_{1/2}^{-1})_1$, (f) $(2p_{3/2}^{-1}3p_{3/2}^{-1})_2$, (g) $(2p_{3/2}^{-1}3p_{3/2}^{-1})_0$, (h) $(2p_{1/2}^{-1}3p_{3/2}^{-1})_1$, (i) $(2p_{1/2}^{-1}3p_{3/2}^{-1})_2$, and (j) $(2p_{1/2}^{-1}3p_{1/2}^{-1})_0$. The structures contributed by the main final configurations are shown in plot (a).

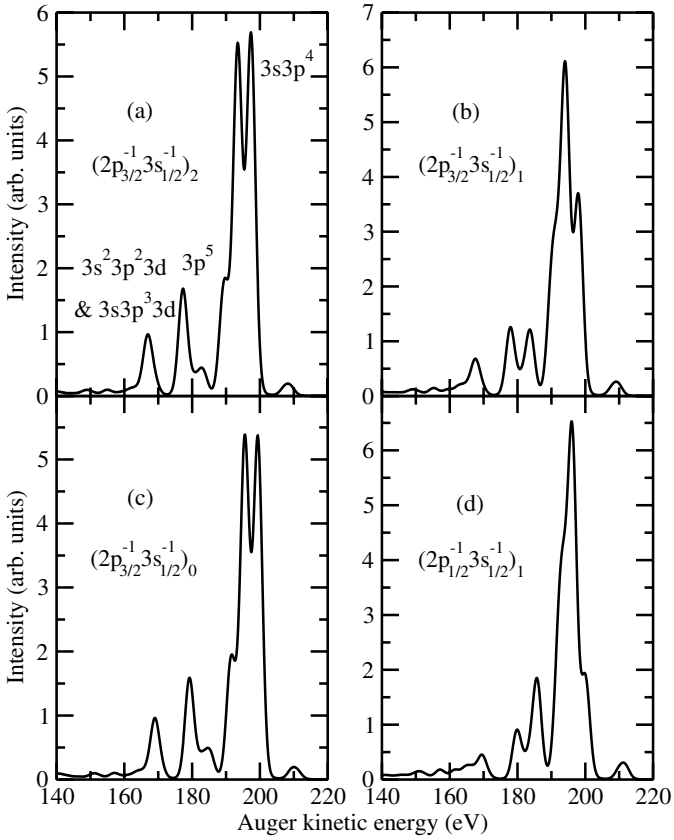

Fig. 2. Auger spectra for the single Auger decay of levels belonging to Ar^{2+} $2p^53s3p^6$ $(2p^{-1}3s^{-1})$ configuration: (a) $(2p_{3/2}^{-1}3s_{1/2}^{-1})_2$, (b) $(2p_{3/2}^{-1}3s_{1/2}^{-1})_1$, (c) $(2p_{3/2}^{-1}3s_{1/2}^{-1})_0$, and (d) $(2p_{1/2}^{-1}3s_{1/2}^{-1})_1$.

the Auger process as the effects of electron correlations become weaker for higher charged ion.

The Auger spectra are shown in Figures 1 and 2 for the decay of levels belonging to the configurations of $2p^53s^23p^5$ and $2p^53s3p^6$, respectively. The spectra are obtained by including the lifetime broadening and an assumed instrument resolution of 3.0 eV full width of half maximum (FWHM) by using a Voigt profile [20]. The main structures from different configurations are depicted in the figure. The relative intensity of the Auger spectra can differ by more than an order of magnitude depending on the individual levels of $2p^53s^23p^5$, yet it is very close for levels of $2p^53s3p^6$. With the increase in the level energy of $2p^53s^23p^5$, the structure of the Auger spectra becomes simpler, which is due to smaller contributions from channels with higher energies. For the five strong autoionized levels (Figs. 1f–1j), there are three distinct structures which are due to channels of $3s^23p^3$, $3s3p^4$ and $3p^5$. However, the contributions from channels of higher energies such as $3s^23p^23d$ and $3s3p^33d$ are evident for the lower energy levels shown in Figures 1a–1e.

The Auger spectra of the configuration averaged results are given in Figures 3 and 4 for $2p^53s^23p^5$ and $2p^53s3p^6$, respectively. In Figures 3a and 4a, only the autoionization widths are considered, while additional instrumental resolution of 3.0 eV FWHM is included in Figures 3b and 4b. The main channels due to different configurations are shown in both figures. Note, however, that some weak structures contributed by configurations of $3p^5$, $3s^23p^23d$ and $3s3p^33d$ are mixed in energy location. Evident difference can be found between plots (a) and (b) in Figures 3 and 4 for the Auger spectra with and without the inclusion of 3.0 eV FWHM instrumental resolution. We chose a resolution of 3.0 eV FWHM from the comparison of our theoretical Auger spectra with the experimental observation of Huttula et al. [11], which will be discussed later. Higher instrumental resolution is needed to clarify more details in the Auger spectra shown in plots (a) of both figures.

Our theoretical work can be utilized to interpret the experimental results of Huttula et al. [11]. These authors proposed an alternative method to measure Auger electron spectroscopy with inner-shell ionization of positively charged ions, which is based on the core valence double photoionization of the neutral species. As a result, the populations of levels belonging to the configurations of

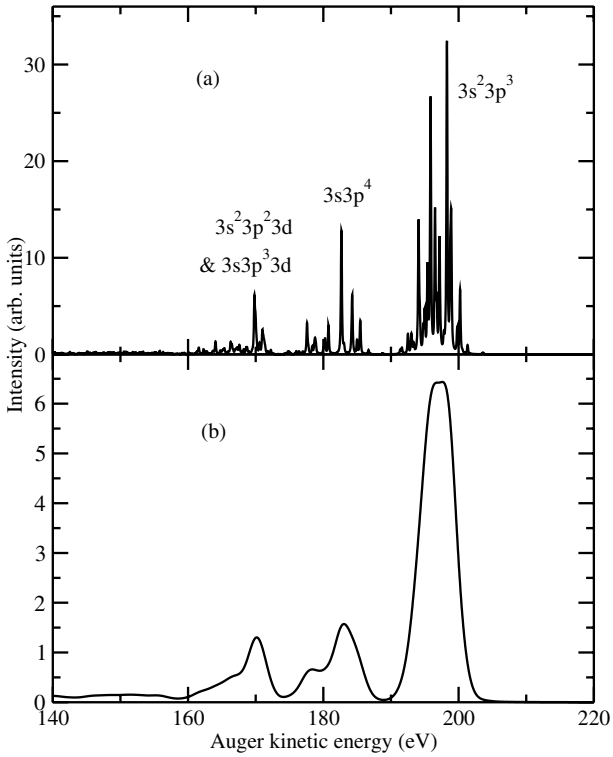

Fig. 3. Auger spectra for the configuration averaged results of Ar^{2+} $2p^53s^23p^5$ ($2p^{-1}3p^{-1}$): (a) only the autoionization widths are considered and (b) additional instrumental resolution of 3.0 eV FWHM is included.

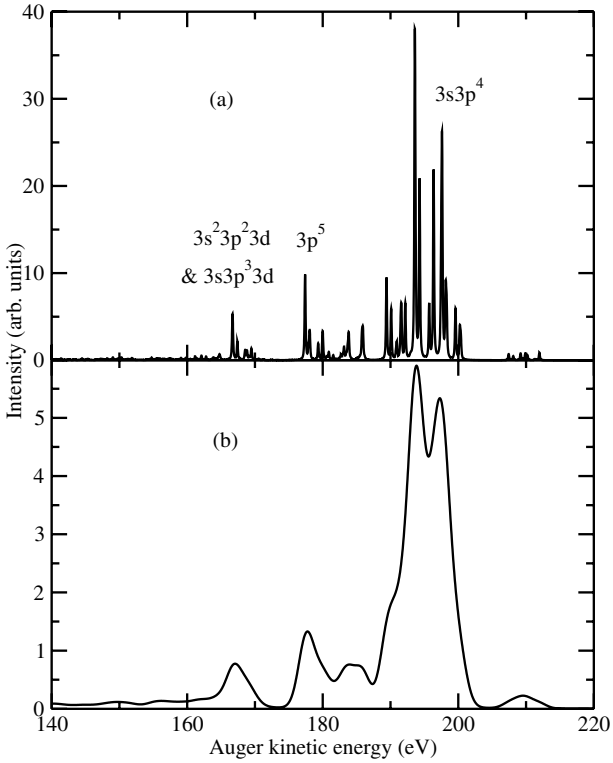

Fig. 4. Auger spectra for the configuration averaged results of Ar^{2+} $2p^53s3p^6$ ($2p^{-1}3s^{-1}$): (a) only the autoionization widths are considered and (b) additional instrumental resolution of 3.0 eV FWHM is included.

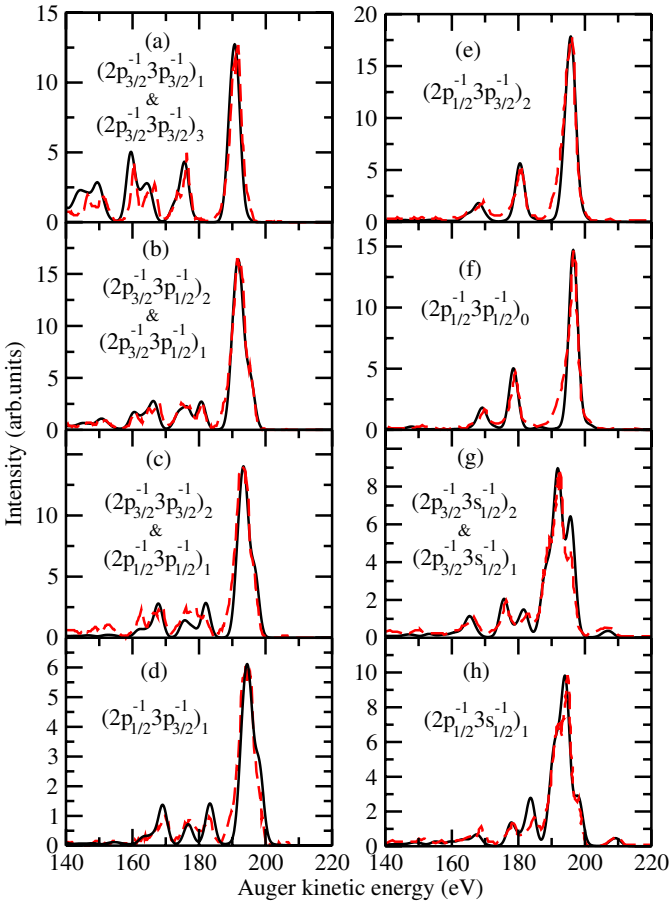

Fig. 5. Comparison of our calculated Auger spectra (solid lines) with the experimental results of Huttula et al. [11] (dashed lines) for selected $2p^{-1}v^{-1}$ ($v = 3p$ and $3s$) states.

$2p^53s^23p^5$ and $2p^53s3p^6$ produced in their experiment are different. In order to compare with the experiment, our calculated Auger spectra shown in Figures 1 and 2 should be multiplied by the population fraction of different levels. This value of fraction is deduced from the measured population counts of Huttula et al. [11]. Our calculated Auger spectra are compared with experimental results in Figure 5. To have a best comparison with experiment, the theoretical Auger kinetic energy is shifted to the lower energy direction by 2 eV. Obviously, we successfully interpreted the experimental results. The main structures for the shown results are in excellent agreement with the experimental observations. Three groups of final levels can be clearly seen in the figure, with the strongest Auger spectra being due to levels of $3s^23p^3$ with the highest Auger kinetic energy and the next strongest one to $3s3p^4$. Our results represent an improvement over the theoretical simulation [11]. All structures are well predicted with adequate precision.

The results shown in the above are restricted to the single Auger decay. There is also possibility for Ar^+ $2p^{-1}$ to decay by the direct double Auger process. To the best of our knowledge, no work was reported, either experimentally or theoretically, on the DDAD process of Ar^+

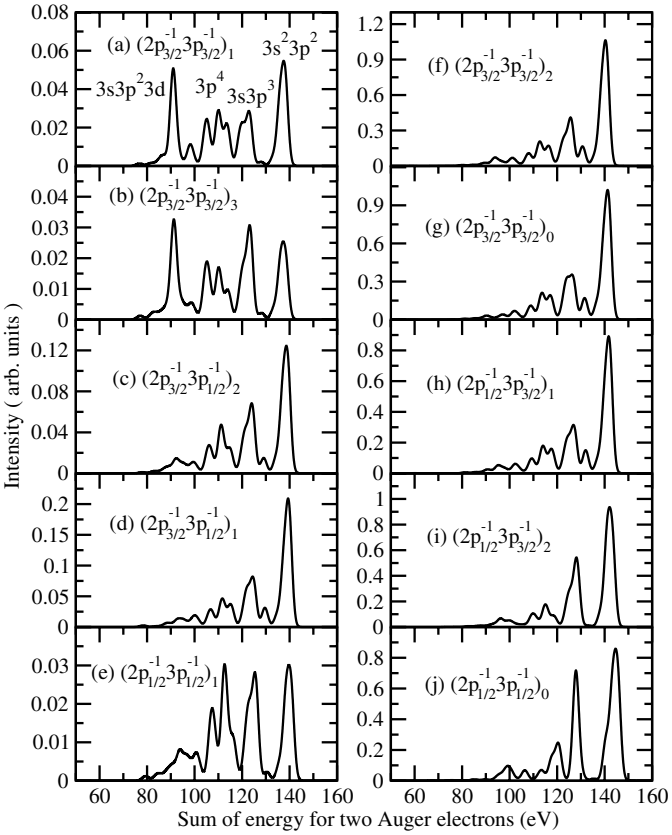

Fig. 6. Auger spectra for the DDAD process of Ar^{2+} levels of $2p^53s^23p^5$. Level designation is the same as in Figure 1.

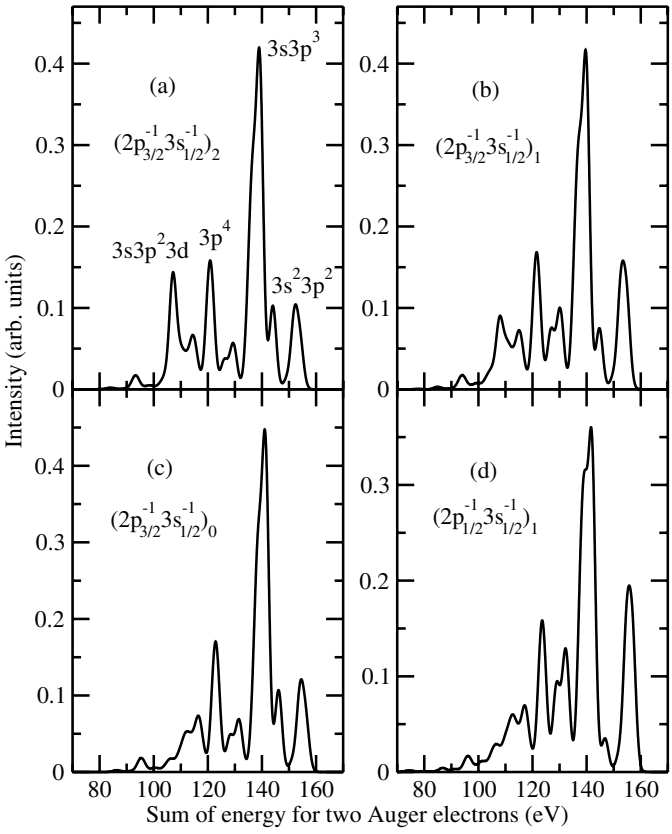

Fig. 7. Auger spectra for the DDAD process of Ar^{2+} levels of $2p^53s3p^6$. Level designation is the same as in Figure 2.

$2p^{-1}$ hole states. The level-to-level DDAD rates are calculated according to the separate mechanisms of the KO and SO and the results are given in Figures 6 and 7 for the levels of $2p^53s^23p^5$ and $2p^53s3p^6$, respectively. The results showed that KO is the dominant DDAD mechanism for the BR of the double Auger decay into states of Ar^{4+}. The Auger spectra are obtained by including the lifetime broadening and an assumed instrument resolution of 3.0 eV FWHM by using a Voigt profile [20,21]. From the inspection of Figures 6 and 7, one can see that four main groups of final DDAD states are clearly visible, which are levels belonging to the configurations of $3s^23p^2$, $3s3p^3$, $3p^4$ and $3s3p^23d$ of Ar^{4+}. For the levels of (f)–(j) shown in Figure 6 with larger DDAD rates, about 50% probability is contributed by the levels of the ground configuration of $3s^23p^2$. Yet for the levels belonging to the configuration of $2p^53s3p^6$, more than 50% probability is contributed by the first excited configuration of $3s3p^3$. It is noted that the levels of $3s3p^23d$ contributed evidently to the DDAD rates for all levels of $2p^53s^23p^5$ and $2p^53s3p^6$, yet that of $3s^23p3d$ is negligibly small. To have a more direct and quantitative understanding for the DDAD channels of Ar^+ $2p^{-1}$, we transformed the level-to-level rates to level-to-configuration rates by summing over all possible final levels belonging to one particular configuration. The corresponding DDAD rates are given in Table 3.

The total single Auger and DDAD rates and BRs of the DDAD to the total Auger process for levels of $2p^53s^23p^5$ and $2p^53s3p^6$ are listed in Table 4. The BRs range from 6.2% to 10.8% for different individual level. The configuration averaged DDAD BRs are 6.5% and 7.3%, respectively, for $2p^53s^23p^5$ and $2p^53s3p^6$. Compared with the Auger decay of Ar $2p^{-1}$ [20], we found different features between Ar and Ar^+ $2p^{-1}$ hole states. First, the Auger decay rates are nearly equivalent for the level resolved single and double processes of Ar $2p^{-1}$, yet the rates of a $2p$ hole in an Ar^+ ($2p^53s^23p^5$) ion can differ by more than an order of magnitude depending on different states, both for the single and double Auger processes. Secondly, the probability of the cascade double Auger process is negligibly trivial for Ar^+ $2p^{-1}$ hole states compared with that of Ar $2p^{-1}$ (2.9%). Levels of Ar $2p^{-1}$ also have larger DDAD probability (12.0%) than those of Ar^+ $2p^{-1}$ (configuration averaged value of 6.5% for $2p^53s^23p^5$ and 7.3% for $2p^53s3p^6$). The theoretical results for Ar $2p^{-1}$ hole states are in good agreement with the experimental measurements [4,5,33]. However, there is no experimental report on the BRs of the double Auger process of Ar^+ $2p^{-1}$ hole states up to now. Further experimental measurements on the complete Auger decay process are needed to better understand this basic process.

4 Conclusion

In conclusion, complete Auger decay including the single and double processes of Ar^+ $2p^{-1}$ hole states are studied

Table 3. Level-to-configuration double decay rates A^2 (s^{-1}) and the BRs for the main channels of Ar^+ $2p^{-1}$ hole states. Figures in brackets indicate powers of ten. The last two columns refer to the DDAD rates (s^{-1}) and BRs (in %) of the main channels.

Level	J	Final config.	A^2	BR (%)
$2p_{3/2}^{-1}3p_{3/2}^{-1}$	1	$3s^23p^2$	7.742 (11)	26.2
		$3s3p^3$	8.067 (11)	27.3
		$3p^4$	2.896 (11)	9.8
		$3s3p^23d$	6.471 (11)	21.9
$2p_{3/2}^{-1}3p_{3/2}^{-1}$	3	$3s^23p^2$	3.861 (11)	17.7
		$3s3p^3$	6.262 (11)	28.7
		$3p^4$	2.378 (11)	10.9
		$3s3p^23d$	5.084 (11)	23.3
$2p_{3/2}^{-1}3p_{1/2}^{-1}$	2	$3s^23p^2$	1.788 (12)	38.2
		$3s3p^3$	1.474 (12)	31.5
		$3p^4$	3.182 (11)	6.8
		$3s3p^23d$	3.791 (11)	8.1
$2p_{3/2}^{-1}3p_{1/2}^{-1}$	1	$3s^23p^2$	2.701 (12)	43.6
		$3s3p^3$	2.056 (12)	33.2
		$3p^4$	3.531 (11)	5.7
		$3s3p^23d$	3.035 (11)	4.9
$2p_{1/2}^{-1}3p_{1/2}^{-1}$	1	$3s^23p^2$	4.636 (11)	21.2
		$3s3p^3$	6.627 (11)	30.3
		$3p^4$	2.296 (11)	10.5
		$3s^23p3d$	3.018 (11)	13.8
		$3s3p^23d$	2.887 (11)	13.2
$2p_{3/2}^{-1}3p_{3/2}^{-1}$	2	$3s^23p^2$	1.410 (13)	49.7
		$3s3p^3$	9.365 (12)	33.0
		$3p^4$	1.391 (12)	4.9
		$3s^23p3d$	1.391 (12)	4.9
		$3s3p^23d$	1.305 (12)	4.6
$2p_{3/2}^{-1}3p_{3/2}^{-1}$	0	$3s^23p^2$	1.463 (13)	50.8
		$3s3p^3$	9.562 (12)	33.2
		$3p^4$	9.792 (11)	3.4
		$3s^23p3d$	1.467 (12)	5.1
		$3s3p^23d$	1.325 (12)	4.6
$2p_{1/2}^{-1}3p_{3/2}^{-1}$	1	$3s^23p^2$	1.219 (13)	49.7
		$3s3p^3$	8.070 (12)	32.9
		$3p^4$	1.104 (12)	4.5
		$3s^23p3d$	1.177 (12)	4.8
		$3s3p^23d$	1.227 (12)	5.0
$2p_{1/2}^{-1}3p_{3/2}^{-1}$	2	$3s^23p^2$	1.291 (13)	49.3
		$3s3p^3$	8.643 (12)	33.0
		$3p^4$	1.021 (12)	3.9
		$3s^23p3d$	1.388 (12)	5.3
		$3s3p^23d$	1.205 (12)	4.6
$2p_{1/2}^{-1}3p_{1/2}^{-1}$	0	$3s^23p^2$	1.253 (13)	48.4
		$3s3p^3$	8.696 (12)	33.6
		$3p^4$	8.799 (11)	3.4
		$3s^23p3d$	1.682 (12)	6.5
		$3s3p^23d$	3.423 (12)	5.5
$2p_{3/2}^{-1}3s_{1/2}^{-1}$	2	$3s^23p^2$	1.518 (12)	10.0
		$3s3p^3$	1.242 (13)	53.9
		$3p^4$	2.231 (12)	14.7
		$3s3p^23d$	2.110 (12)	13.9
$2p_{3/2}^{-1}3s_{1/2}^{-1}$	1	$3s^23p^2$	2.072 (12)	13.5
		$3s3p^3$	8.105 (12)	52.8
		$3p^4$	2.072 (12)	13.5
		$3s3p^23d$	1.704 (12)	11.1
$2p_{3/2}^{-1}3s_{1/2}^{-1}$	0	$3s^23p^2$	1.533 (12)	11.0
		$3s3p^3$	8.057 (12)	57.8
		$3p^4$	2.007 (12)	14.4
		$3s3p^23d$	1.129 (12)	8.1
$2p_{1/2}^{-1}3s_{1/2}^{-1}$	1	$3s^23p^2$	2.564 (12)	16.9
		$3s3p^3$	7.767 (12)	51.2
		$3p^4$	1.927 (12)	12.7
		$3s3p^23d$	1.335 (12)	8.8

Table 4. Single Auger decay rates A^1, DDAD rates A^2 (sum of KO and SO mechanisms) and ion number ratios (INR) (%) of the direct double to total Auger decay rates of the levels of $2p^{-1}v_s^{-1}(v_s = 3s, 3p)$. Figures in brackets indicate powers of ten. The last two lines refer to the configuration averaged results of the INR of the double to total probability including the single and DDAD processes.

Level	J	A^1	A^2	INR(%)
$2p_{3/2}^{-1}3p_{3/2}^{-1}$	1	3.098 (13)	2.955 (12)	9.5
$2p_{3/2}^{-1}3p_{3/2}^{-1}$	3	2.014 (13)	2.182 (12)	10.8
$2p_{3/2}^{-1}3p_{1/2}^{-1}$	2	6.269 (13)	4.680 (12)	7.5
$2p_{3/2}^{-1}3p_{1/2}^{-1}$	1	8.965 (13)	6.194 (12)	6.9
$2p_{1/2}^{-1}3p_{1/2}^{-1}$	1	2.206 (13)	2.187 (12)	9.9
$2p_{3/2}^{-1}3p_{3/2}^{-1}$	2	4.531 (14)	2.838 (13)	6.3
$2p_{3/2}^{-1}3p_{3/2}^{-1}$	0	4.668 (14)	2.880 (13)	6.2
$2p_{1/2}^{-1}3p_{3/2}^{-1}$	1	3.905 (14)	2.453 (13)	6.3
$2p_{1/2}^{-1}3p_{3/2}^{-1}$	2	4.190 (14)	2.619 (13)	6.3
$2p_{1/2}^{-1}3p_{1/2}^{-1}$	0	4.099 (14)	2.588 (13)	6.3
$2p_{3/2}^{-1}3s_{1/2}^{-1}$	2	2.045 (14)	1.518 (13)	7.4
$2p_{3/2}^{-1}3s_{1/2}^{-1}$	1	2.078 (14)	1.535 (13)	7.4
$2p_{3/2}^{-1}3s_{1/2}^{-1}$	0	2.006 (14)	1.394 (13)	7.0
$2p_{1/2}^{-1}3s_{1/2}^{-1}$	1	2.084 (14)	1.540 (13)	7.4
$2p^{-1}3p^{-1}$		2.013 (14)	1.316 (13)	6.5
$2p^{-1}3s^{-1}$		2.060 (14)	1.517 (13)	7.3

by using a distorted wave method in the theoretical framework of perturbation. For the levels belonging to the configuration of $2p^53s^23p^5$, both the single Auger and direct double Auger decay rates differ by more than an order of magnitude. The predicted lifetime widths range from ∼10 meV to ∼300 meV, but the lifetime widths are nearly equivalent for the levels of $2p^53s3p^6$. Our theoretical spectra of the single Auger decay process nicely explained a recent experiment by using a novel method based on core valence photoionization of the neutral Ar. To obtain such a good agreement, it is necessary to include adequate electron correlations in a large scale CI calculation and to keep a balanced description of the electron correlations between the initial Ar^+ $2p^{-1}$ hole states and those of the Auger

decay pathways. The relative intensity of all structures shown in the Auger spectra agree well with experiment. For direct double Auger decay, the contribution from the KO mechanism dominates over that of shake-off. The DDAD rates are determined in the level-to-level and level-to-configuration formalism. For the stronger autoionized levels of $2p^5 3s^2 3p^5$, ∼50% double decay probability is contributed by the ground configuration $3s^2 3p^2$ of Ar^{4+}. Yet more than 50% probability is due to the first excited configuration $3s3p^3$ of Ar^{4+} for the levels of $2p^5 3s3p^6$. The configuration averaged BRs of the DDAD to the total rate are predicted to be 6.5% and 7.3%, respectively, for the configurations of $2p^5 3s^2 3p^5$ and $2p^5 3s3p^6$. Further experimental work is needed to investigate the direct double Auger decay of Ar^+ $2p^{-1}$ hole states.

This work was supported by the National Natural Science Foundation of China under Grant Nos. 11274382, 11274383 and 11204376.

References

1. T.R. Kallman, P. Palmeri, Rev. Mod. Phys. **79**, 79 (2007)
2. J.Y. Dai, Y. Hou, J.M. Yuan, Phys. Rev. Lett. **104**, 245001 (2010)
3. U. Alkemper, J. Doppelfeld, F. von Busch, Phys. Rev. A **56**, 2741 (1997)
4. S. Brünken, Ch. Gerth, B. Kanngießer, T. Luhmann, M. Richter, P. Zimmermann, Phys. Rev. A **65**, 042708 (2002)
5. J. Viefhaus et al., Phys. Rev. Lett. **92**, 083001 (2004)
6. S. Namba, N. Hasegawa, M. Nishikino, T. Kawachi, M. Kishimoto, K. Sukegawa, M. Tanaka, Y. Ochi, K. Takiyama, K. Nagashima, Phys. Rev. Lett. **99**, 043004 (2007)
7. R. Guillemin et al., Phys. Rev. Lett. **109**, 013001 (2012)
8. J.M. Bizau, D. Cubaynes, M. Richter, F.J. Wuilleumier, J. Obert, J.C. Putaux, T.J. Morgan, E. Källne, S. Sorensen, A. Damany, Phys. Rev. Lett. **67**, 576 (1991)
9. S. Al Moussalami, J.M. Bizau, B. Rouvellou, D. Cubaynes, L. Journel, F.J. Wuilleumier, J. Obert, J.C. Putaux, T.J. Morgan, M. Richter, Phys. Rev. Lett. **76**, 4496 (1996)
10. A. Gottwald, Ch. Gerth, M. Richter, Phys. Rev. Lett. **82**, 2068 (1999)
11. S.M. Huttula, P. Lablanquie, L. Andric, J. Palaudoux, M. Huttula, S. Sheinerman, E. Shigemasa, Y. Hikosaka, K. Ito, F. Penent, Phys. Rev. Lett. **110**, 113002 (2013)
12. W. Ackermann et al., Nat. Photon. **1**, 336 (2007)
13. P. Emma et al., Nat. Photon. **4**, 641 (2010)
14. L. Young et al., Nature **466**, 56 (2010)
15. S.M. Vinko et al., Nature **482**, 59 (2012)
16. B. Rudek et al., Nat. Photon. **6**, 858 (2012)
17. H. Fukuzawa et al., Phys. Rev. Lett. **110**, 173005 (2013)
18. L.J. Frasinski et al., Phys. Rev. Lett. **111**, 073002 (2013)
19. W.J. Xiang, C. Gao, Y.S. Fu, J.L. Zeng, J.M. Yuan, Phys. Rev. A **86**, 061401(R) (2012)
20. J.L. Zeng, P.F. Liu, W.J. Xiang, J.M. Yuan, Phys. Rev. A **87**, 033419 (2013)
21. J.L. Zeng, P.F. Liu, W.J. Xiang, J.M. Yuan, J. Phys. B **46**, 215002 (2013)
22. M.S. Pindzola, D.C. Griffin, Phys. Rev. A **36**, 2628 (1987)
23. M.F. Gu, Can. J. Phys. **86**, 675 (2008)
24. M.Ya. Amusia, I.S. Lee, V.A. Kilin, Phys. Rev. A **45**, 4576 (1992)
25. P. Lablanquie, S.M. Huttula, M. Huttula, L. Andric, J. Palaudoux, J.H.D. Eland, Y. Hikosaka, E. Shigemasa, K. Ito, F. Penent, Phys. Chem. Chem. Phys. **13**, 18355 (2011)
26. F.A. Parpia, C.F. Fischer, I.P. Grant, Comput. Phys. Commun. **94**, 249 (1996)
27. C.F. Fritzsche, J. Electron Spectrosc. Related Phenom. **114-116**, 1155 (2001)
28. C.F. Fritzsche, C.F. Fischer, G. Gaigalas, Comput. Phys. Commun. **148**, 103 (2002)
29. J.L. Zeng, J.M. Yuan, Phys. Rev. E **74**, 025401(R) (2006)
30. J.L. Zeng, J.M. Yuan, Phys. Rev. E **76**, 026401 (2007)
31. J.L. Zeng, J. Phys. B **41**, 125702 (2008)
32. J.L. Zeng, C. Gao, J.M. Yuan, Phys. Rev. E **82**, 026409 (2010)
33. M. Nakano, Y. Hikosaka, P. Lablanquie, F. Penent, S.M. Huttula, I.H. Suzuki, K. Soejima, N. Kouchi, K. Ito, Phys. Rev. A **85**, 043405 (2012)